

# Data-driven, structure-based hyperelastic manifolds: A macro-micro-macro approach

Víctor Jesús Amores, José María Benítez, Francisco Javier Montáns\*

*Escuela Técnica Superior de Ingeniería Aeronáutica y del Espacio  
Universidad Politécnica de Madrid  
Plaza Cardenal Cisneros, 3, 28040-Madrid, Spain*

---

## Abstract

In this paper we introduce a novel approach to obtain the stored energy of rubber-like materials directly from experimental data. The model is structure-based, in which the only assumption is the existence of an isotropic distribution of fibres, chains or networks. Using a single macroscopic test, we obtain the response of the constituents solving a system of equations. This response includes all possible interactions, without an assumption on the nature of that behavior, performing reverse-engineering of the constituents behavior. With that microstructural behavior, we build constitutive manifolds capable of reproducing accurately the behavior of the continuum under any arbitrary loading condition. To demonstrate the goodness of the proposed non-parametric macro-micro-macro approach, using just one of the macroscopic test curves of the Kawabata experiments to compute the fiber (micro) behavior, we reproduce to very good accuracy the rest of the series of biaxial tests from Kawabata. We show similar results for the Treloar material. With the use of constitutive manifolds, the method has similar efficiency in finite element programs to that of analytical models.

*Keywords:* Rubber-like materials, hyperelasticity, macro-micro-macro approach, data-driven modeling, constitutive manifolds.

---

## 1. Introduction

The behavior of polymeric-like materials, including elastomers and soft biological tissues, is characterized by a highly nonlinear elastic behavior capable of developing very large strains without dissipating a relevant amount energy [1, 2, 3, 4, 5]. As a consequence of this conservative behavior, these materials are modeled as hyperelastic materials by assuming

---

\*Corresponding author

Email address: `fco.montans@upm.es` (Francisco Javier Montáns )

the existence of a potential function, also called strain energy function [2, 5]. The mathematical setting of the potential has been traditionally performed inferring an analytical function shape, a shape which accommodates experimental evidence through some material parameters. These material parameters are determined by fitting the model predictions to the experimental data from the material by means of nonlinear optimization techniques. Depending on whether, or not, the behavior of the constituents are explicitly included in the formulation, the hyperelastic models can be classified respectively in structure-based models and phenomenological models.

The main advantage of the phenomenological (macro) approach is that there is no need to make assumptions on the microstructure or its behavior. However, the accuracy of these models under general deformations depends on the selected analytical shape and on the number of material parameters. In general, these models require a larger number of experimental data than the structure-based ones, and result in increased complexity for increased accuracy. Hence, data-driven approaches have been proposed to increase the generality in modelling and to incorporate data in a more direct manner [6, 7, 8]. Within the phenomenological framework, and grounded on the Sussman-Bathe model for isotropic, incompressible materials [9], our group has developed a new non-parametric data-driven approach where neither an analytical shape of the energy function nor material parameters are considered. Due to the data-driven conception and the ability to accurately capture experimental data, we named the new framework as WYPiWYG (What-You-Prescribe-is-What-You-Get) hyperelasticity. WYPiWYG hyperelasticity is a procedure that, instead of fitting, *solves* numerically the equilibrium differential equations that govern a determined test, obtaining the material behavior for more general cases. The stored energy density is obtained interpolating the resulting values by splines or B-splines. WYPiWYG hyperelasticity has been successfully applied to anisotropic materials [10, 11], compressible materials [12], and unconventional materials [13]. In all these cases, the proposed models have been able to reproduce smooth experimental tests to any desired precision. The similar accuracy has been found for general loading cases [14] or when WYPiWYG models have been implemented in finite element codes [12, 15]. In the case of noisy experiments, some stability conditions may be guaranteed when they are needed [16].

On the other hand, structure-based models take into account the molecular structure of the material by means of functions and material parameters related to that micro-structure, so it is a micro-macro approach. The most common procedure is based on statistical mechanics considering the chains as freely joined chains composed of  $N$  segments of equal length, called Khun segments. Each Khun segment has a length  $l$ , so the length of the chain is  $L = Nl$ . The chain is assumed rigid and coiled but free to rotate, keeping the internal energy unchanged. In order to determine the work of deformation of every single chain, the difference in the configurational entropy between the unstretched and stretched states is determined. Assuming no intermolecular interaction, the stored energy is obtained by the sum of the energy stored in each chain [4, 5]. One of the best-known models of this kind is the 8-chain affine model developed by Arruda and Boyce. The reason for the

success of this model is that with only two material parameters, easily obtained from a tensile test, the model is capable of reproducing the behavior of isotropic incompressible materials to acceptable accuracy as shown in [17] for the Treloar tests [18]. However, when obtaining the parameters from a tensile test, the stresses for the equibiaxial test are underestimated. Miehe et al. [19] argued that this underestimation was due to the unconstrained assumption of the chains. Following similar ideas as in the extended tube model [20], in their non-affine microsphere model they constrained the movement of a single chain assuming it embedded in a micro-tube. This constraint and non-affinity insert three material parameters additional to those of the 8-chain model (5 in total). To determine them, three Treloar tests were needed [19], therefore loosing the main asset of the Arruda-Boyce model. Furthermore, in these non-affine microsphere models, the macroscopic strain energy function is obtained considering the chains continuously distributed and integrating the strain energy of the chains over the unit sphere. Recently, Khiêm and Itskov observed that the results of this kind of models depended on the numerical integration scheme [21], so to avoid numerical integration they developed a micro-macro mechanical model based on the network-averaging of the tube model with a closed-form of the Rayleigh non-Gaussian distribution. This model was formulated with four material parameters but, again, the set of three experimental tests by Treloar were needed to determine them. As they noted, citing Urayama [22], it is believed that several tests are needed to capture the influence of the two invariants (or, say, chain behavior and constraint effect).

In this paper a new non-parametric data-driven macro-micro-macro approach is proposed for modeling isotropic hyperelastic materials. The only assumption made is the existence of a network of chains/fibers. No conjecture about the origin of the behavior of the chains is made. No analytical form, nor material parameters, are assumed for that behavior. With the experimental data of a single test, the proposed procedure calculates the energy function of a single chain solving a linear system of equations. The macroscopic behavior is reproduced by the integration of the stored energy of each chain in a unit sphere accounting for the isotropic distribution of the chains. Since it is a data-driven model, it implicitly captures the effects of the interactions between fibers, cross-linking and stress-induced crystallization at large strains without any explicit assumption. Pre-integrated macroscopic manifolds may be easily built from the computed micromechanical behavior, so the implementation in finite element codes is standard, straightforward, and as efficient as that of phenomenological models.

The macro-micro-macro approach presented in this paper entails a new framework to model hyperelastic materials. Whereas in the classical micro-macro approach followed by structure-based models, material parameters are used to best-fit the *assumed* chain entropic behavior, in this macro-micro-macro approach we *solve* numerically for the actual behavior of the fiber with the single assumption of an isotropic distribution. As a clear advantage of this approach, we only need one test, whereas as mentioned, using the classical micro-macro approach the authors usually report to need several sets of experimental data (see e.g. section 6.4 of [19] and section 3.1 of [21]).

To show the performance of the new procedure, we apply it below to the test series by Kawabata et al. [23] and Treloar [18]. As remarked by Khiêm and Itskov [21] very few models are able to reproduce with acceptable accuracy the experiments from Kawabata et al [23]. However, all these models need more than one test to obtain the material parameters. Khiêm and Itskov and Marckmann and Verron further noted that the Kawabata et al and the Treloar material are the same material, so the model parameters for the latter should predict the former experiments, an ability which only the models by Kaliske and Heinrich [20], Shariff [24], Miehe et al. [19] and their own proposal have. We show that with our proposal: (1) we are able to predict to excellent accuracy the experiments of Kawabata et al [23] using only the information of one experimental curve to calibrate the material; (2) we are able to predict the experiments of Treloar using the information of a single Treloar test; and (3) that the model calibrated with the Treloar material predicts to good accuracy the experiments of Kawabata et al [23], but that both materials do not behave in an identical manner.

## 2. About chain models and their pre-integration

The behavior of the chains in structure-based polymer models frequently follow statistical mechanics approaches. Initial Gaussian treatments evolved into more accurate Langevin statistical treatments to account for the locking stretch when the distance between chain ends  $r_{ch} \rightarrow Nl$ . These models require the evaluation of the inverse of the Langevin function  $\mathcal{L}^{-1}(r_{ch}/Nl) = y$ , where  $\mathcal{L}(y) = \coth(y) - 1/y$  is the Langevin function. Considering Langevin-based statistics, the probability distribution  $\mathbf{p}(r_{ch})$  gives the following chain entropy [4]

$$s(r_{ch}) = k \ln \mathbf{p}(r_{ch}) = k \left[ c - N \left( \frac{r_{ch}}{Nl} y + \ln \frac{y}{\sinh y} \right) \right] \quad (1)$$

where  $k$  is the Boltzmann constant and  $c$  is another constant. The stretch of the chain is  $\lambda_{ch} = r_{ch}/r_0 = r_{ch}/(\sqrt{N}l)$ , which reaches a locking value of  $\lambda_{lock} = \sqrt{N}$ . Then, neglecting changes in internal energy as usual in these models, the tension in the chain can be obtained from the thermodynamic requirement

$$F_{ch}(r_{ch}) = -T \frac{ds(r_{ch})}{dr_{ch}} = \frac{kT}{l} \mathcal{L}^{-1} \left( \frac{\lambda_{ch}}{\sqrt{N}} \right) \quad (2)$$

where  $T$  is the absolute temperature, and the nominal stress is

$$P_{ch}(r_{ch}) = -T \frac{ds(\lambda_{ch})}{d\lambda_{ch}} = F_{ch}(r_{ch}) \frac{dr_{ch}}{d\lambda_{ch}} = \sqrt{N}l F_{ch}(r_{ch}) \quad (3)$$

For small values of  $r_{ch}/Nl$ , the Gaussian description is recovered because by Taylor series

$$\mathcal{L}^{-1}(r_{ch}/Nl) \simeq 3 \frac{r_{ch}}{Nl} = 3 \frac{\lambda_{ch}}{\sqrt{N}} + \dots \quad (4)$$

so  $F_{ch}(\lambda_{ch}) = 3l^{-1}kT\lambda_{ch}/\sqrt{N}$ ; for a more detailed explanation see [25]. Note that for Langevin-based models, if  $\lambda_{ch} \rightarrow \lambda_{lock}$ , then  $\mathcal{L}^{-1}(\lambda_{ch}/\sqrt{N}) \rightarrow \mathcal{L}^{-1}(1) \rightarrow \infty$ , so  $P_{ch}(\lambda_{ch}) \rightarrow \infty$ , whereas the Gaussian approach provides load values linear with the stretch.

Models based on Langevin statistics are conceptually appealing, but have some limitations that should be beared in mind. The first one is the accurate evaluation of the inverse Langevin function itself. Since there is no known closed form, and accuracy in the evaluation is extremely important [26], several approximants have been proposed in the last years [27, 28, 29, 30, 31, 32]. Comparisons are given in [30] and [33]. The most accurate approximant is given in [33], using a spline-based approach. A better alternative to the use of the Langevin function is given recently by Khiêm and Itskov [21] using the Rayleigh distribution function, resulting in a closed-form of the exact non-Gaussian probability distribution. In fact, the inverse Langevin function accurately represents the probability distribution only when  $N$  is large enough (large chains, about  $N = 25 \sim 50$ , see for example discussion around Figs. 6.3 and 6.6 in [4]), but the values obtained from fitting to macroscopic tests may be near this value; see e.g. Figs 11 and 14 in [17]. The second limitation is the purely entropic treatment of the stored energy, because it is well-known that stress-induced crystallization is relevant in some polymers at large strains, so the internal energy may have a considerable contribution; see for example Fig. 1.9 in [4], Fig. 3.5 of [34], Figs 3 and 4 in [35] and references [36, 37].

As mentioned, one of the best known models of this kind is the 8-chain model, which has only two parameters, namely  $G = nkT$  (where  $n$  is the chain density) and  $N$ , easily obtained from a tensile test or other alternative test. With the information obtained from that test, relatively good predictions are obtained for other loading modes. The 8-chain model considers a microstructure of 8 chains, being the diagonals of a regular hexahedron oriented according to the principal directions of deformation. All 8 chains suffer the same microstructural (affine) stretch  $\bar{\lambda}_{ch}$  under any continuum deformation. Considering an arbitrary direction in spherical coordinates —see Fig. 1

$$\mathbf{r} = r_1 \mathbf{N}_1 + r_2 \mathbf{N}_2 + r_3 \mathbf{N}_3 = \sin \phi \cos \theta \mathbf{N}_1 + \sin \phi \sin \theta \mathbf{N}_2 + \cos \phi \mathbf{N}_3 \quad (5)$$

where  $\mathbf{N}_i$  are the principal directions of deformation in the reference configuration, the affine squared stretch in direction  $\mathbf{r}$  is  $\lambda_{ch}^2 = (\mathbf{r} \otimes \mathbf{r}) : \mathbf{C}$ , where  $\mathbf{C} = \mathbf{X}^T \mathbf{X}$  is the right Green-Cauchy deformation tensor and  $\mathbf{X}$  is the deformation gradient. If we integrate  $\lambda_{ch}^2$  over a sphere  $S$  we have, after some algebra [25], that the mean squared stretch is the same

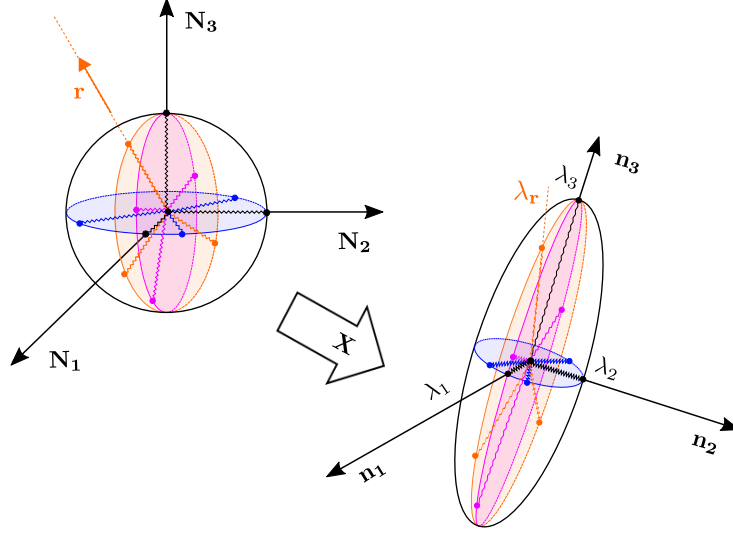


Figure 1: Affine deformation of the unit sphere.

as the squared stretch in each one of the 8 chains of the Arruda-Boyce model:

$$\frac{1}{S} \int_S \lambda_{ch}^2 dS = \frac{\lambda_1^2 + \lambda_2^2 + \lambda_3^2}{3} = \frac{I_1}{3} = \bar{\lambda}_{ch}^2 \quad (6)$$

Thus,  $\bar{\lambda}_{ch} = \sqrt{I_1/3}$ , where  $I_1$  is the first principal invariant of the Cauchy-Green deformation tensor  $\mathbf{C}$ . Since we have the functional dependence  $\bar{\lambda}_{ch}(I_1)$ , this function may be inserted in Eq. (2) to obtain the derivative of the stored energy density of the continuum  $d\Psi(I_1)/dI_1$  upon consideration of a chain density of  $n$ ; see [17] for more details. However, if we assume that the stored energy may be written in the form  $\Psi(\lambda_1, \lambda_2, \lambda_3) = \Psi(I_1) = \Psi(\bar{\lambda}_{ch})$  –note the abuse of notation to avoid the proliferation of symbols–, a WYPiWYG approach may be adopted, so the prescribed data is exactly captured without the need of considering the statistical treatment. Furthermore, if the 8-chain structure is adopted, the average chain behavior can also be obtained without considering the probability distribution; see [25]. Noteworthy, the prescribed data (from a single test) may be captured to any precision, but as with the Arruda-Boyce model, the model fails to accurately predict the behavior for all deformation modes. As explained in [25], the reason is that an 8-chain configuration considers only a single continuum variable (i.e. the first invariant), but the possible continuum deformation modes of an isotropic incompressible material have two degrees of freedom. For instance, the ratio between the  $I_2$  invariant and the  $I_1$  invariant changes substantially from the uniaxial and pure shear deformations to the equibiaxial deformations, see Fig. 11 in [25]. Therefore an accurate constitutive model must include the two macroscopic degrees of freedom, even though the microscopic behavior in an isotropic

material could be characterized by a single variable.

Since the first invariant represents only the mean squared stretch and filters the influence of the deviations from that mean value, the second invariant, along with the couplings between both invariants, must be present in the higher order moments. Generally for any direction of the space we can write the squared stretch as the addition of the mean value and the deviation from that mean value

$$\lambda_{ch}^2 = \bar{\lambda}_{ch}^2 + \delta_{ch} \quad (7)$$

where  $\delta_{ch} = \lambda_{ch}^2 - \bar{\lambda}_{ch}^2$  and by definition

$$\int_S \delta_{ch} dS = 0 \quad (8)$$

Thus, the quantity  $\delta_{ch}$  represents the deviation. The diagonals of the cube in the eight chain model are average directions of the sphere in terms of  $\lambda_{ch}^2$  (they happen to have always the mean squared stretch). It is important to note that  $\frac{1}{S} \int_S \Psi^*(\lambda_{ch}^2) dS \neq \Psi^*(\bar{\lambda}_{ch}^2)$  and  $\frac{1}{S} \int_S \Psi^*(\delta_{ch}) dS \neq \Psi^*(0)$ ; i.e. the average energy or the average of the stresses are not those obtained from an average stretch measure. The accuracy of the results provided by the eight chain model in particular, and the relevance of using average strain measures in general, can be understood by the following Taylor expansion centered on  $\bar{\lambda}_{ch}^2$ .

$$\Psi^*(\lambda_{ch}^2) = \Psi^*(\bar{\lambda}_{ch}^2 + \delta_{ch}) = \Psi^*(\bar{\lambda}_{ch}^2) + \left. \frac{d\Psi^*(x)}{dx} \right|_{x=\bar{\lambda}_{ch}^2} \delta_{ch} + \frac{1}{2} \left. \frac{d^2\Psi^*(x)}{dx^2} \right|_{x=\bar{\lambda}_{ch}^2} \delta_{ch}^2 + \dots \quad (9)$$

This expression may be integrated in the sphere to give the continuum, macroscopic energy. Note that the quantities  $\Psi^*(\bar{\lambda}_{ch}^2)$ ,  $d\Psi/dx|_{\bar{\lambda}_{ch}^2}$ ,  $d^2\Psi/dx^2|_{\bar{\lambda}_{ch}^2}$  are constant within the integral. Then, using Eq. (8), after some lengthy but straightforward algebra, we arrive at

$$\frac{1}{S} \int_S \Psi^*(\lambda_{ch}^2) dS = \underbrace{\Psi^*(\bar{\lambda}_{ch}^2)}_{\text{eight-chain model}} + 0 + \underbrace{\left. \frac{d^2\Psi^*(x)}{dx^2} \right|_{\bar{\lambda}_{ch}^2} \frac{2}{45} (I_1^2 - 3I_2) + \left. \frac{d^3\Psi^*(x)}{dx^3} \right|_{\bar{\lambda}_{ch}^2} I_{\delta 6}}_{\text{terms not taken into account by eight-chain model}} + \dots \quad (10)$$

where  $I_{\delta 6}$  is an invariant function of 6<sup>th</sup> order powers of the stretches. Noteworthy, this is a pre-integrated expression in which the first term  $\Psi^*(\bar{\lambda}_{ch}^2) = \Psi^*(I_1)$ —recall the abuse of notation—contains the stored energy of an 8-chain model and the second term containing  $d\Psi^*/dx$  vanishes identically. The first appearance of the second invariant is in the third term of the series. Including this term, the pursued different relation between the uniaxial and the equibiaxial tests is obtained. However, the subsequent terms of the series become increasingly important away from the reference state, when the stretch  $\lambda_{ch}^2$  of the fibers is

not close to the mean value  $\bar{\lambda}_{ch}^2$ , i.e. when  $\delta_{ch} \gg 0$ . This is expected in rubber-like solids under general deformations. If we insist in using an average strain and only the first term of the series, we are in fact embedding the information of the remaining terms in that single term when fitting experiments. However, the relation between terms change considerably for different tests, so they should be included explicitly in computing the stored energy  $\Psi = \frac{1}{S} \int_S \Psi^* dS$ .

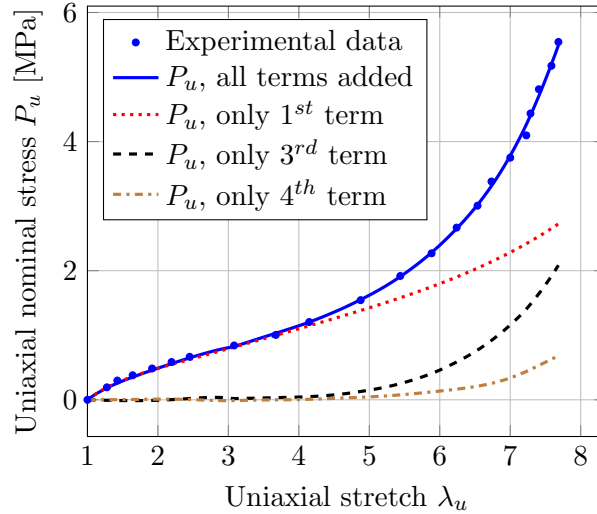


Figure 2: Nominal stress,  $P_u$  computed with a WYPiWYG procedure including up to the fourth term of Taylor's expansion of a pre-integrated scheme.

A WYPiWYG procedure can be applied to Eq. (10) to obtain the macroscopic stored energy  $\Psi = \frac{1}{S} \int_S \Psi^* dS$  by considering spline interpolations for  $\Psi^*(x)$  and retaining several terms. In Fig. 2 we show such a computation retaining up to the 4<sup>th</sup> term, and we plot the influence of each term in the sum. Of course, the procedure is capable of capturing the uniaxial test to high accuracy regardless of the number of terms considered. However, the higher order terms will have a different influence in other types of tests; note for example that the third term in Eq. (10) includes the second invariant. The problem of such approach is that whereas the high order terms vanish for small strains, at large strain may even become dominant, as the tendency in Fig. 2 shows. In line with the number of series terms needed for an accurate evaluation of the inverse Langevin function [29], unfortunately, the number of terms in the series of Eq. (10) that need to be considered is high, so such a procedure is expensive and the interpolation functions should be derivable as many times, complicating the procedure.



### 3. Proposed macro-micro-macro approach

From the observations in the previous section, it seems difficult to obtain an accurate procedure following a macroscopic fitting of a pre-integrated scheme, which is the approach followed by some models, among them, the Arruda-Boyce model. For this reason, we pursue a different macro-micro-macro approach, in which instead of interpolating a pre-integrated expression, we interpolate the fiber function itself and push up that interpolation to the continuum level. Then, the nodal values of the microstructural behavior are obtained solving a linear system of equations at the continuum level, fully determining the needed micro-mechanical behavior. Thereafter, with this micro-mechanical behavior, constitutive manifolds may be construed to determine the behavior of the continuum under any arbitrary deformation directly at that level, without the need of performing numerical integration at the micro level.

Therefore, our proposal only assumes the existence of chain/fiber-like (or network-like) elementary structures isotropically distributed in the solid, whose elongation or shortening at the micro-scale level determines the behaviour of the continuum at the macroscopic level. We assume that the behavior of all fibers is the same, i.e.  $\tilde{\Psi}_{ch}(\lambda_{ch})$ . Then, given the stretch of every single chain/fiber  $i$  in the solid,  $\lambda_{ch_i}$ , it is possible to obtain the macroscopic stored energy density function,  $\Psi(\lambda_1, \lambda_2, \lambda_3)$ . Conversely, if that one-to-one relation holds, it is in general possible to determine the behavior of the representative chain, including all chain interactions, from a single macroscopic test. This is possible because the behavior of the chain depends on a single variable  $\lambda_{ch}$ , and all chains are equal, and isotropically distributed. Furthermore, since all interactions are included and the functional relation is open (it will be determined below), we can assume an *affine* relation for  $\lambda_{ch}$  as  $\lambda_{ch}(\lambda_1, \lambda_2, \lambda_3, \theta, \phi)$ , where  $\theta$  and  $\phi$  are the spherical angles giving the orientation of the fiber respect to the principal directions of deformations. Under the affinity assumption, any sphere in the continuum will be deformed according to the principal stretches, see Fig. 1. From Figure 1, it is obvious that the stretch in any arbitrary direction of the sphere is

$$\lambda_{ch} = (\mathbf{r} \otimes \mathbf{r}) : \mathbf{U} = \lambda_1 \sin^2 \phi \cos^2 \theta + \lambda_2 \sin^2 \phi \sin^2 \theta + \lambda_3 \cos^2 \phi = \lambda_1 r_1^2 + \lambda_2 r_2^2 + \lambda_3 r_3^2 \quad (11)$$

where  $\mathbf{U} = \sqrt{\mathbf{C}}$  is the stretch tensor. Considering the number of chains in a sphere  $n_{ch}$ , the density of chains per volume unit is  $\rho = n_{ch}/V$ , where  $V$  is the volume of the sphere (e.g.  $\frac{4}{3}\pi$ ). The energy density of the continuum is

$$\Psi(\lambda_1, \lambda_2, \lambda_3) = \int_V \rho \tilde{\Psi}_{ch}(\lambda_{ch}) dV = \frac{1}{V} \int_V \Psi_{ch}(\lambda_{ch}) dV = \frac{1}{S} \int_S \Psi_{ch}(\lambda_{ch}) dS \quad (12)$$

where  $S$  is the surface of the sphere (e.g.  $4\pi$ ) and  $\Psi_{ch}(\lambda_{ch}) := n_{ch} \tilde{\Psi}_{ch}(\lambda_{ch})$ . If we determine

the stored energy density, the nominal stress for an incompressible isotropic material is:

$$P_i = \frac{1}{\lambda_i} p + \frac{\partial \Psi(\lambda_1, \lambda_2, \lambda_3)}{\partial \lambda_i} \quad (13)$$

where  $p$  is the pressure-like Lagrange multiplier. Using the chain rule, the derivative of the stored energy is

$$\frac{\partial \Psi(\lambda_1, \lambda_2, \lambda_3)}{\partial \lambda_i} = \frac{1}{S} \int_S \frac{\partial \Psi_{ch}(\lambda_{ch})}{\partial \lambda_{ch}} \frac{\partial \lambda_{ch}}{\partial \lambda_i} dS = \frac{1}{S} \int_S P_{ch}(\lambda_{ch}) \frac{\partial \lambda_{ch}(\lambda_1, \lambda_2, \lambda_3, \mathbf{r})}{\partial \lambda_i} dS \quad (14)$$

where  $\mathbf{r}(\theta, \phi)$  gives the direction of each chain/fiber.

Now, our purpose is to determine numerically the function  $P_{ch}(\lambda_{ch})$  directly from data of a macroscopic test, for example a tensile test. In order to do so, consider the following spline-based interpolation

$$P_{ch}(\lambda_{ch}) = \sum_{i=1}^{nv} N_i(\lambda_{ch}) \hat{P}_{chi} = [N_1(\lambda_{ch}) \quad \cdots \quad N_{nv}(\lambda_{ch})] \begin{bmatrix} \hat{P}_{ch1} \\ \vdots \\ \hat{P}_{chnv} \end{bmatrix} \quad (15)$$

where  $nv$  is the number of vertices which have prescribed abscissae  $\hat{\lambda}_{ch1}, \dots, \hat{\lambda}_{chnv}$ , which limits are computed from the available range in the tests and Eq. (11), and corresponding ordinate values  $\hat{P}_{ch1}, \dots, \hat{P}_{chnv}$ , to be computed in this procedure. The functions  $N_i(\lambda_{ch})$  are the interpolation functions, e.g. the B-splines in the present case. If we introduce the expression for  $P_{ch}(\lambda_{ch})$  in Eq. (15) we obtain

$$\frac{\partial \Psi(\lambda_1, \lambda_2, \lambda_3)}{\partial \lambda_i} = \frac{1}{S} \int_S \left( \sum_{m=1}^{nv} N_m(\lambda_{ch}(\lambda_1, \lambda_2, \lambda_3, \mathbf{r})) \hat{P}_{chm} \right) \frac{\partial \lambda_{ch}(\lambda_1, \lambda_2, \lambda_3, \mathbf{r})}{\partial \lambda_i} dS \quad (16)$$

where we have left explicit the dependencies for the reader's convenience.

The sphere integral can be computed numerically using a Gaussian quadrature. The one used here, proposed by Bazant and Oh [38], has  $nq$  number of quadrature points (in the examples below we use the case  $nq = 21$ , the same one used for example by Miehe et al. in their non-affine model [19]):

$$\frac{1}{S} \int_S f(\mathbf{r}) dS \simeq \sum_{j=1}^{nq} f(\mathbf{r}_j) w_j \quad (17)$$

so

$$\frac{\partial \Psi(\lambda_1, \lambda_2, \lambda_3)}{\partial \lambda_i} = \sum_{j=1}^{nq} w_j \frac{\partial \lambda_{ch}(\lambda_1, \lambda_2, \lambda_3, \mathbf{r}_j)}{\partial \lambda_i} \sum_{m=1}^{nv} N_m(\lambda_{ch}(\lambda_1, \lambda_2, \lambda_3, \mathbf{r}_j)) \hat{P}_{ch_m} \quad (18)$$

Write for simplicity  $\lambda_{ch}(\lambda_1, \lambda_2, \lambda_3, \mathbf{r}_j) =: \lambda_{chj}$  and note that by Eq. (11) we have the relation  $\partial \lambda_{ch}(\lambda_1, \lambda_2, \lambda_3, \mathbf{r}_j) / \partial \lambda_i = r_{ji}^2$ , which is the square of the  $i$ -th component of the vector  $\mathbf{r}_j$  (at integration point  $j$  of the quadrature). Since the vector of B-spline vertices  $\hat{P}_{ch_k}$  is constant, it can be factored-out from the sum. Then we can write the sum in  $m = 1, \dots, nv$  in matrix notation as

$$\frac{\partial \Psi(\lambda_1, \lambda_2, \lambda_3)}{\partial \lambda_i} = \begin{bmatrix} \sum_{j=1}^{nq} r_{ji}^2 w_j N_1(\lambda_{chj}) & \cdots & \sum_{j=1}^{nq} r_{ji}^2 w_j N_{nv}(\lambda_{chj}) \end{bmatrix} \begin{bmatrix} \hat{P}_{ch_1} \\ \vdots \\ \hat{P}_{ch_{nv}} \end{bmatrix} \quad (19)$$

which can be written in compact form as

$$\frac{\partial \Psi(\lambda_1, \lambda_2, \lambda_3)}{\partial \lambda_i} = \sum_{j=1}^{nq} r_{ji}^2 [\text{row}_N(\lambda_{chj})] \begin{bmatrix} \hat{P}_{ch_1} \\ \vdots \\ \hat{P}_{ch_{nv}} \end{bmatrix} \quad (20)$$

where  $[\text{row}_N(\lambda_{chj})] = w_j [N_1(\lambda_{chj}) \cdots N_{nv}(\lambda_{chj})]$ . Now, as an example (a similar procedure is obtained for any other test), using Eq. (13) for the case of a biaxial test in the 1-2 plane ( $P_1, P_2, P_3 = 0$ ):

$$P_1 = \frac{\partial \Psi(\lambda_1, \lambda_2, \lambda_3)}{\partial \lambda_1} - \frac{\lambda_3}{\lambda_1} \frac{\partial \Psi(\lambda_1, \lambda_2, \lambda_3)}{\partial \lambda_3} = \sum_{j=1}^{nq} \left( r_{j1}^2 - r_{j3}^2 \frac{\lambda_3}{\lambda_1} \right) [\text{row}_N(\lambda_{chj})] \begin{bmatrix} \hat{P}_{ch_1} \\ \vdots \\ \hat{P}_{ch_{nv}} \end{bmatrix} \quad (21)$$

This equation is established for as many points as desired from the experimental data. In practice, from experimental data points, a spline function  $P_1(\lambda_1)$  can be built, and as many points as desired may be obtained by sampling the spline function. Consider an uniaxial test or a test with  $\lambda_2$  fixed. Taking  $nl$  points with uniaxial stretches  $\hat{\lambda}_{u1}, \dots, \hat{\lambda}_{unl}$  (note that we need  $nl > nv$ ), and corresponding nominal stresses  $P_1(\hat{\lambda}_i)$ , the previous equation takes the form

$$\begin{bmatrix} P_1(\lambda_1 = \hat{\lambda}_{u1}) \\ \vdots \\ P_1(\lambda_1 = \hat{\lambda}_{unl}) \end{bmatrix} \simeq \begin{bmatrix} P_1^{Bs}(\lambda_1 = \hat{\lambda}_{u1}) \\ \vdots \\ P_1^{Bs}(\lambda_1 = \hat{\lambda}_{unl}) \end{bmatrix} \equiv \begin{bmatrix} \bar{N}_{1,1} & \cdots & \bar{N}_{1,nv} \\ \vdots & \cdots & \vdots \\ \bar{N}_{nl,1} & \cdots & \bar{N}_{nl,nv} \end{bmatrix} \begin{bmatrix} \hat{P}_{ch_1} \\ \vdots \\ \hat{P}_{ch_{nv}} \end{bmatrix} \quad (22)$$

where  $P_1(\hat{\lambda}_i)$  are the values from the experimental curve for stretches  $\hat{\lambda}_u$  and  $P_1^{Bs}(\lambda_1 = \hat{\lambda}_{ui})$  are the corresponding model continuum values obtained from the computed B-spline representing the chain behavior. The coefficients  $\bar{N}_{i,j}$  of the matrix are

$$\bar{N}_{i,j} = \sum_{q=1}^{nq} \left( r_{q1}^2 - r_{q3}^2 \frac{\lambda_3(\hat{\lambda}_{ui})}{\hat{\lambda}_{ui}} \right) w_q N_j(\lambda_{chq}(\hat{\lambda}_{ui})) \quad (23)$$

The previous system of equations is rectangular (usually  $nl \gg nv$ ), and it can be written in the following compact form:

$$\mathbf{P}_1^{Bs}(\hat{\lambda}_u) = \bar{\mathbf{N}}(\hat{\lambda}_u) \hat{\mathbf{P}}_{ch} \quad (24)$$

Then, we minimize the quadratic error between the values obtained from experimental points,  $\mathbf{P}_1(\hat{\lambda}_u)$ , and the estimation computed from the nodal values of the stress in the chains,  $\mathbf{P}_1^{Bs}(\hat{\lambda}_u)$ . The function is

$$g(\hat{\mathbf{P}}_{ch}) = \frac{1}{2} \left[ \mathbf{P}_1^{Bs}(\hat{\lambda}_1) - \mathbf{P}_1(\hat{\lambda}_1) \right]^T \mathbf{W} \left[ \mathbf{P}_1^{Bs}(\hat{\lambda}_1) - \mathbf{P}_1(\hat{\lambda}_1) \right] \quad (25)$$

where the design variables, to be obtained, are  $\hat{\mathbf{P}}_{ch}$ . In the above expression we included a diagonal matrix  $\mathbf{W}$  to weight, if needed, the errors of the different experimental data.

Experimental data is usually not smooth, but we consider that the model should give smooth stress-strain behavior. Then, a smoothing procedure should also be included. The smoothness of the curve can be controlled using a penalization in the second derivative and stability conditions (increasing load in the chain for increasing stretch) can be guaranteed using a penalization in the first derivative in case it is negative. There are many algorithms for spline smoothing (see [39]). Since this discussion is not the purpose of the present manuscript, we just mention a simple effective procedure employing approximate derivatives using finite differences of the vertices (i.e. a P-splines approach, see [40])

$$D_j^{(1)} = \frac{\hat{P}_{ch,j+1} - \hat{P}_{ch,j}}{h} = \frac{1}{h} (\hat{P}_{ch,j+1} - \hat{P}_{ch,j}) \quad (26)$$

$$D_j^{(2)} = \frac{D_{j+1}^{(1)} - D_j^{(1)}}{h} = \frac{1}{h^2} (\hat{P}_{ch,j+2} - 2\hat{P}_{ch,j+1} + \hat{P}_{ch,j}) \quad (27)$$

$$D_j^{(3)} = \frac{D_{j+1}^{(2)} - D_j^{(2)}}{h} = \frac{1}{h^3} (\hat{P}_{ch,j+3} - 3\hat{P}_{ch,j+2} + 3\hat{P}_{ch,j+1} - \hat{P}_{ch,j}) \quad (28)$$

where  $h = \Delta\lambda_{ch}$  is the size of each interval in the spline. These finite differences are used to build the corresponding matrices  $\mathbf{D}^{(k)}$  containing the coefficients of  $\hat{\mathbf{P}}_{ch}$ . The penalty

terms are added to build the function to be minimized

$$\min_{\hat{\mathbf{P}}_{ch}} \left\{ \frac{1}{2} \hat{\mathbf{P}}_{ch}^T \bar{\mathbf{N}}^T \mathbf{W} \bar{\mathbf{N}} \hat{\mathbf{P}}_{ch} - \hat{\mathbf{P}}_{ch}^T \bar{\mathbf{N}}^T \mathbf{W} \mathbf{P}_1 + \frac{1}{2} \hat{\mathbf{P}}_{ch}^T \mathbf{D}^{(1)T} \boldsymbol{\Omega}^{(1)} \mathbf{D}^{(1)} \hat{\mathbf{P}}_{ch} \right. \\ \left. + \frac{1}{2} \hat{\mathbf{P}}_{ch}^T \mathbf{D}^{(2)T} \boldsymbol{\Omega}^{(2)} \mathbf{D}^{(2)} \hat{\mathbf{P}}_{ch} + \frac{1}{2} \hat{\mathbf{P}}_{ch}^T \mathbf{D}^{(3)T} \boldsymbol{\Omega}^{(3)} \mathbf{D}^{(3)} \hat{\mathbf{P}}_{ch} \right\} \quad (29)$$

where  $\boldsymbol{\Omega}^{(k)}$  is a diagonal weighting matrix to increase/decrease the smoothing in some parts, if desired. The system of equations is

$$\mathbf{A} \hat{\mathbf{P}}_{ch} = \mathbf{b} \quad (30)$$

where

$$\mathbf{A} = \bar{\mathbf{N}}^T \mathbf{W} \bar{\mathbf{N}} + \mathbf{D}^{(1)T} \boldsymbol{\Omega}^{(1)} \mathbf{D}^{(1)} + \mathbf{D}^{(2)T} \boldsymbol{\Omega}^{(2)} \mathbf{D}^{(2)} + \mathbf{D}^{(3)T} \boldsymbol{\Omega}^{(3)} \mathbf{D}^{(3)} \quad (31)$$

$$\mathbf{b} = \bar{\mathbf{N}}^T \mathbf{W} \mathbf{P}_1 \quad (32)$$

Smoothing parameters may guarantee, when needed, smoothness and stability conditions directly imposed on  $P_{ch}(\lambda_{ch})$ . The smoothing parameters may take default values, be prescribed by the user, or automatically computed. Some techniques for automatic spline smoothing are also widely known, see e.g. [41, 42], but are not relevant to the discussion in this paper, so we do not elaborate further.

Once the spline function  $P_{ch}(\lambda_{ch})$  representing the behavior of the typical chain is known, the behavior of the continuum under a general deformation mode, characterized by  $\lambda_1, \lambda_2, 1/(\lambda_1 \lambda_2)$  in an incompressible material, can be determined using Eq. (19). In practice, constitutive manifolds for  $\partial \Psi(\lambda_1, \lambda_2, \lambda_3)/\partial \lambda_i$  may be used for efficient evaluation in a finite element program, so computational times are similar to those employing analytical phenomenological models as, for example, Ogden's model. These manifolds are constructed evaluating the derivatives for a grid  $\{\hat{\lambda}_1, \hat{\lambda}_2\} \in [\lambda_{1min}, \lambda_{1max}] \times [\lambda_{2min}, \lambda_{2max}]$  and fitting a bidimensional spline. For example, following the typical finite element procedure [3], the bidimensional manifolds can be written as

$$\frac{\partial \Psi(\lambda_1, \lambda_2)}{\partial \lambda_1} =: \Psi_1(\lambda_1, \lambda_2) = \sum_{I=1}^{NP} N_I^\square(\lambda_1, \lambda_2) \hat{\Psi}_{1I} \quad (33)$$

where  $N_I^\square(\lambda_1, \lambda_2) = N_i(\lambda_1) N_j(\lambda_2)$  are the bi-dimensional functions obtained as the tensor product of the one-dimensional spline functions  $N_i$ ,  $I(i, j)$  is the typical table of indices and  $\hat{\Psi}_{1I}$  are the vertices of the bi-dimensional spline. Of course the manifolds may be constructed also in terms of the principal invariants  $I_1, I_2$

## 4. Examples

### 4.1. Predictions for the Kawabata experiments

One of the most challenging experimental sets on rubber-like materials are the Kawabata biaxial experiments. Kawabata performed biaxial tests on vulcanized rubber containing 8 phr sulfur. In these biaxial tests, they prescribed different fixed stretches  $\lambda_1$  in one direction, varying the stretch  $\lambda_2$  in the other in-plane direction. During each test, they measured the nominal stresses  $P_1$  and  $P_2$  in both directions, hence obtaining two families of curves, namely  $P_1(\lambda_1, \lambda_2)$  and  $P_2(\lambda_1, \lambda_2)$ . Since the material behaves in a quasi-incompressible manner, and hence any deformation mode may be characterized with only two independent variables (e.g. either  $\lambda_1, \lambda_2$  or  $I_1, I_2$ ), the Kawabata families of curves represent the behavior of the material in any deformation mode in the range of the prescribed stretches.

Our procedure is a macro-micro-macro procedure, meaning that from the macroscopically observed behavior during a test, using the known material structure, we obtain the behavior of the microstructural components that results in the prescribed macroscopic behavior. Then, since that micro-structural behavior fully describes the macroscopic behavior, it is used to obtain the continuum behavior under any other deformation mode.

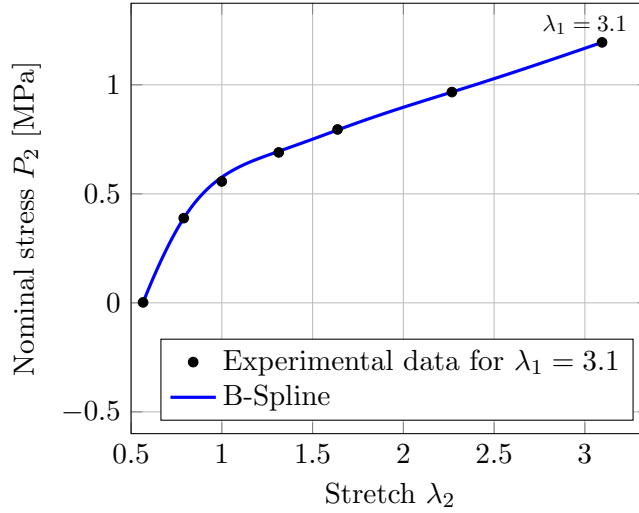


Figure 3: Experimental data employed to compute  $P_{ch}(\lambda_{ch})$  for the Kawabata et al material. Black points are the experimental data for  $\lambda_1 = 3.1$ . The continuous curve is a B-spline capturing those points.

To compute the representative micro-structural behavior of Kawabata's material, *we will just use one of the stress-strain curves from those tests*, in particular the  $\{\lambda_2, P_2\}$  points for  $\lambda_1 = 3.1$ , see Fig. 3. Using the above procedure, solving the system of equations, we obtain the  $\hat{P}_{ch}$  values and then we build a B-spline using those points to have the continuous function  $P_{ch}(\lambda_{ch})$  which represents the behavior of the typical chain of the material; this

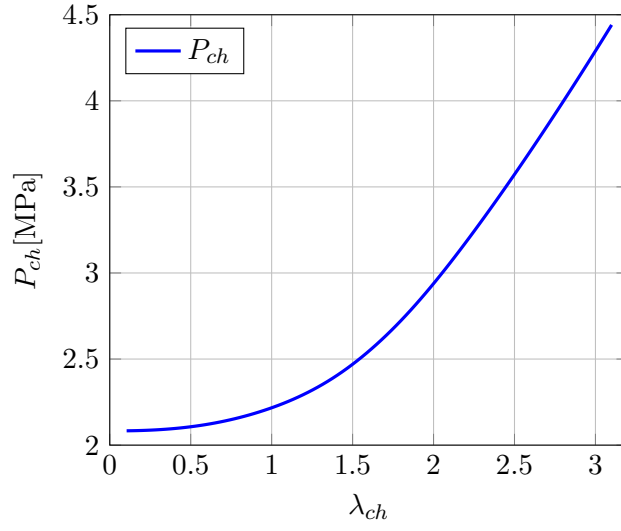


Figure 4:  $P_{ch}(\lambda_{ch})$  obtained from Kawabata's experimental data  $P_2(\lambda_2)$  with  $\lambda_1 = 3.1$

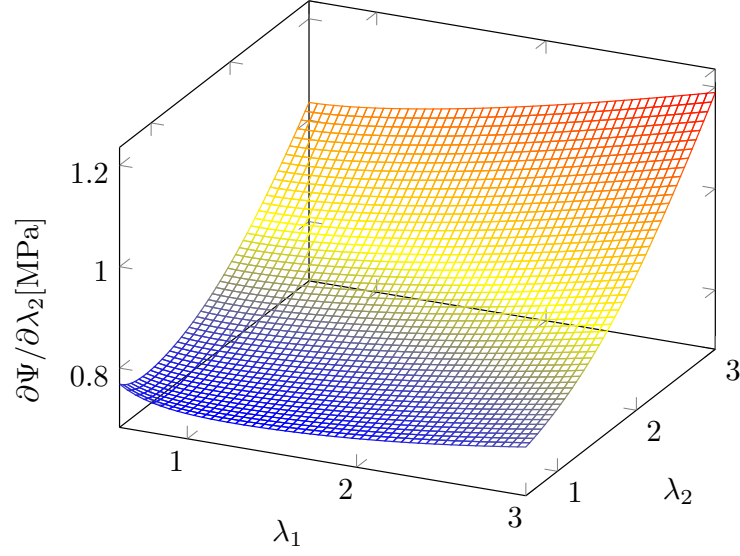


Figure 5: Constitutive manifold obtained from Kawabata's curve  $P_2(\lambda_2)$  with  $\lambda_1 = 3.1$

function is shown in Fig. 4. With that function, we can compute the behavior of the material for any arbitrary deformation mode. For instance, we can compute the constitutive manifold  $\partial\Psi(\lambda_1, \lambda_2, \lambda_3 = (\lambda_1\lambda_2)^{-1})/\partial\lambda_1$ , which is shown in Fig. 5. We note that upon the knowledge of one manifold, for example  $\partial\Psi(\lambda_1, \lambda_2, \lambda_3)/\partial\lambda_1$ , the rest of them may be determined by isotropy requirements, e.g,

$$\frac{\partial\Psi\left(\lambda_1 = \hat{\lambda}_1, \lambda_2 = \hat{\lambda}_2, \lambda_3 = \hat{\lambda}_3\right)}{\partial\lambda_1} = \frac{\partial\Psi\left(\lambda_1 = \hat{\lambda}_2, \lambda_2 = \hat{\lambda}_1, \lambda_3 = \hat{\lambda}_3\right)}{\partial\lambda_2}$$

Using either these manifolds or integrating numerically, we can compute the behavior of the material for the different combinations of  $\lambda_1, \lambda_2$  in the Kawabata experiments, and hence obtain predictions of the  $P_1(\lambda_1, \lambda_2), P_2(\lambda_1, \lambda_2)$  experimental data. Note that we can also build the manifolds  $P_1(\lambda_1, \lambda_2)$  and  $P_2(\lambda_1, \lambda_2)$  to obtain immediately the stress for any loading condition with the constrains of incompressible and plane stress already enforced. Since Kawabata's curves for the biaxial tests are plotted for varying  $\lambda_2$  in the abscissae, for reference we label Axis-2 as longitudinal and Axis-1 as transverse. In Figures 6 and 7 we show the comparison of our predictions for the longitudinal nominal stress  $P_2(\lambda_2)$  with the experimental data from Kawabata et al for different fixed values of transverse stretch  $\lambda_1$ . It is seen that even though we used only one test curve to obtain  $P_{ch}(\lambda_{ch})$ , the predictions are very accurate for all the values of  $\lambda_1$  and  $\lambda_2$ . Furthermore, in Figures 8 and 9 we show the transverse nominal stresses for the same tests, i.e.  $P_1(\lambda_2)$  for the same fixed values of transverse stretch  $\lambda_1$ . These curves show similar accuracy.

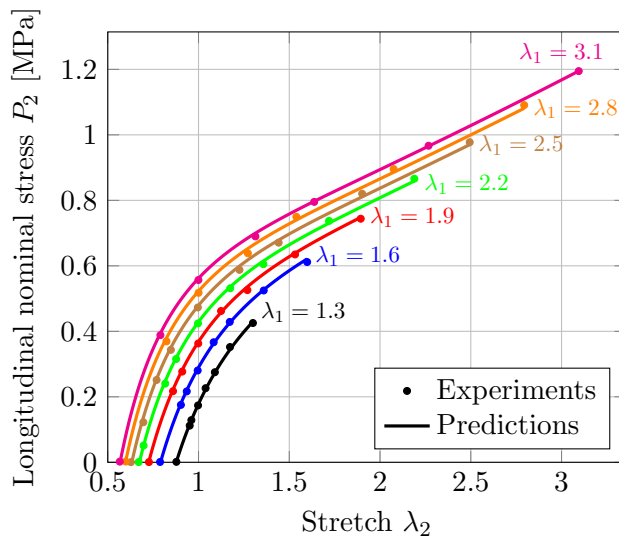


Figure 6: Predictions for the longitudinal nominal stress  $P_2(\lambda_2)$  obtained with the present model for the range  $\lambda_1$  from  $\lambda_1 = 1.3$  to  $\lambda_1 = 3.1$



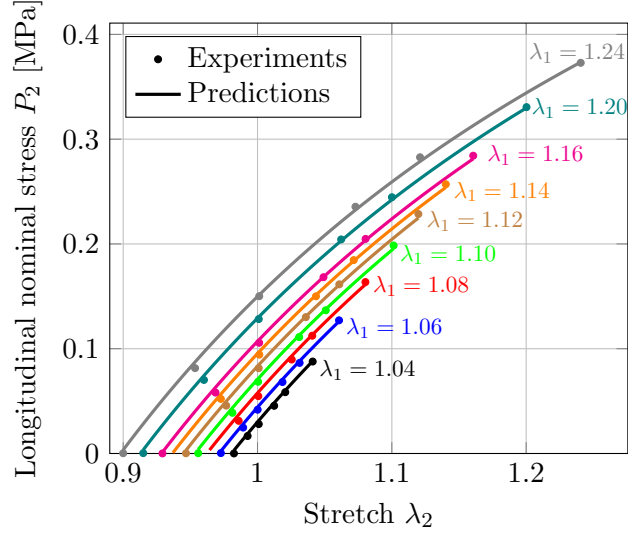


Figure 7: Predictions for  $P_2(\lambda_2)$  obtained with the present model for the range  $\lambda_1$  from  $\lambda_1 = 1.04$  to  $\lambda_1 = 1.24$

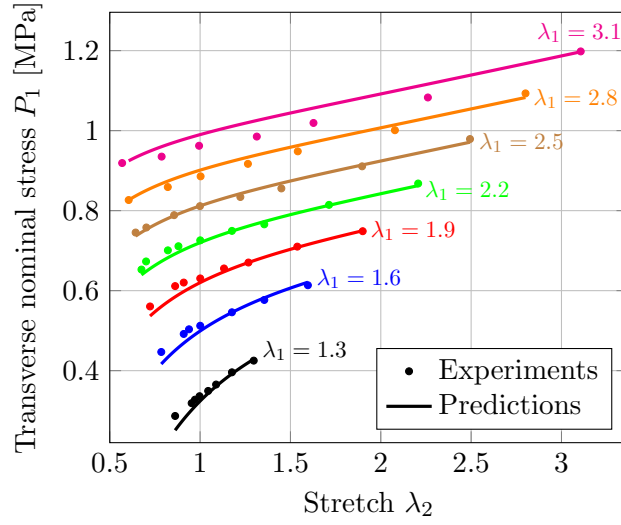


Figure 8: Predictions for  $P_1(\lambda_2)$  obtained with the present model for the range  $\lambda_1$  from  $\lambda_1 = 1.3$  to  $\lambda_1 = 3.1$

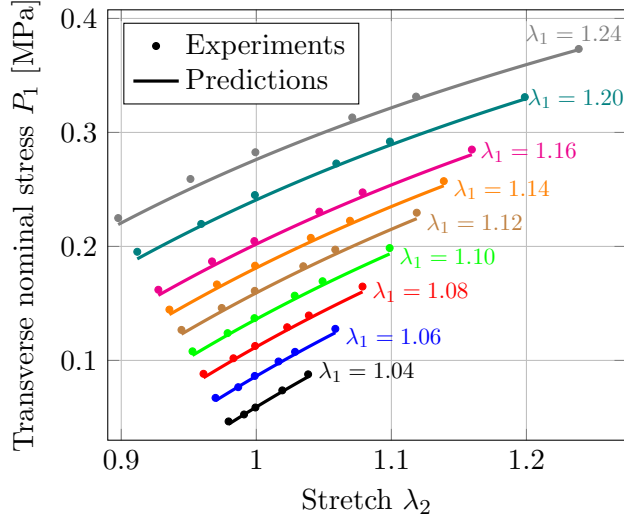


Figure 9: Predictions for  $P_1(\lambda_2)$  obtained with the present model for the range  $\lambda_1$  from  $\lambda_1 = 1.04$  to  $\lambda_1 = 1.24$

To compute the material parameters of their model for the Kawabata et al material, Khiêm and Itskov used three curves (uniaxial, equibiaxial and pure shear) from Treloar's test. They obtained very good predictions for all sets of tests and noted that both materials are in essence the same material. However, following Urayama [22], and because of the issues explained in Sec. 2, they noted the need of using all three tests from Treloar's experiments to calibrate their model, which contained terms in the two principal invariants. In practice, even being micro-mechanically motivated, the model contains two intrinsic degrees of freedom, meaning that it is defined by two different functions of two invariants, each one with its own material parameters, see Eq. (25) in Ref. [21]. In contrast, our model takes full advantage of the assumed structure of the material, as composed of fibers isotropically distributed. Remarkably, no further assumption is made, and the material behavior is fully characterized by a scalar function  $P_{ch}(\lambda_{ch})$ , so it has only one degree of freedom as the Arruda-Boyce model. Then, as we have done for the Kawabata material, the material behavior may be fully determined from a single test as in the Arruda-Boyce model. The only limitation is that to avoid extrapolations, the test must be performed to a sufficient range of stretch, so the obtained  $P_{ch}(\lambda_{ch})$  determines the behavior for all the desired deformations (i.e. these do not exceed the computed  $\lambda_{ch}$  range). Of course extrapolations may be used appending, for example, a rational function with an estimated locking stretch. Furthermore, global analytical functions, instead of P-splines, could be used to fit the microstructural behavior data  $\{\lambda_{ch}, P_{ch}\}$

The Khiêm and Itskov predictions in Fig. 4 of Ref. [21] for the Kawabata et al experiments, using Treloar's curves for calibrating the model, are accurate, but our predictions

for the Kawabata experiments in Figs. 6 and 7, using one of their curves to calibrate the model, are even more accurate. However, the reason maybe that the material from Kawabata and the material from Treloar, having the same chemical composition have slightly different behavior. To investigate this, we will obtain the function  $P_{ch}(\lambda_{ch})$  from Treloar's tests and apply the result to Kawabata's experiments.

#### 4.2. $P_{ch}(\lambda_{ch})$ from the Treloar experiments

Treloar made a well-known series of tests. The uniaxial tensile test, the equibiaxial test and the pure shear test are widely used to verify constitutive models of rubbers. In principle, just one test would be sufficient to characterize  $P_{ch}(\lambda_{ch})$ , and using this function, all tests should be predicted accurately. However, unfortunately the larger stretch reached during the tensile test does not cover all the domain in which  $P_{ch}(\lambda_{ch})$  is evaluated during the equibiaxial test, and vice-versa, the equibiaxial stretch values define a  $P_{ch}(\lambda_{ch})$  domain which does not fully cover the domain needed for the tensile test by Treloar. Then, two options are possible.

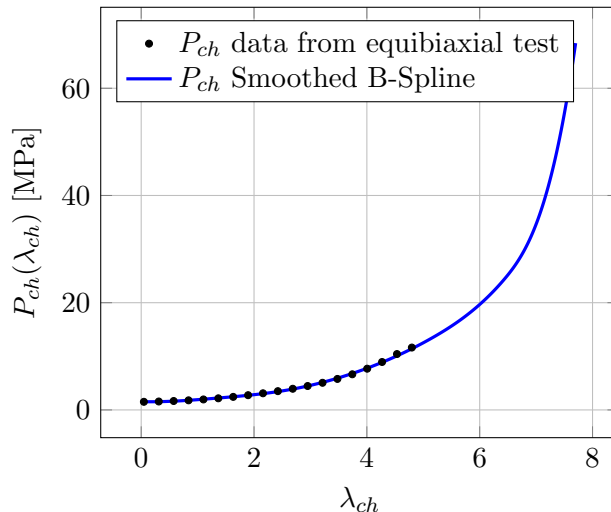


Figure 10:  $P_{ch}$  obtained from an equibiaxial test and extended with a rational function

The first one is to insist in using just one test, for example the equibiaxial test, to characterize the material. Then,  $P_{ch}(\lambda_{ch})$  must be extrapolated in the parts of the domain accessed by the other tests but that were out of range during the equibiaxial test (or a global function may be fitted to the  $P_{ch}(\lambda_{ch})$  data). Such approach is shown in Fig. 10, where the function  $P_{ch}(\lambda_{ch})$  is extrapolated by a rational function of the type

$$f(\lambda_{ch}) = \frac{a\lambda_{ch} + b}{\lambda_{lock}^2 - \lambda_{ch}^2} \quad (34)$$

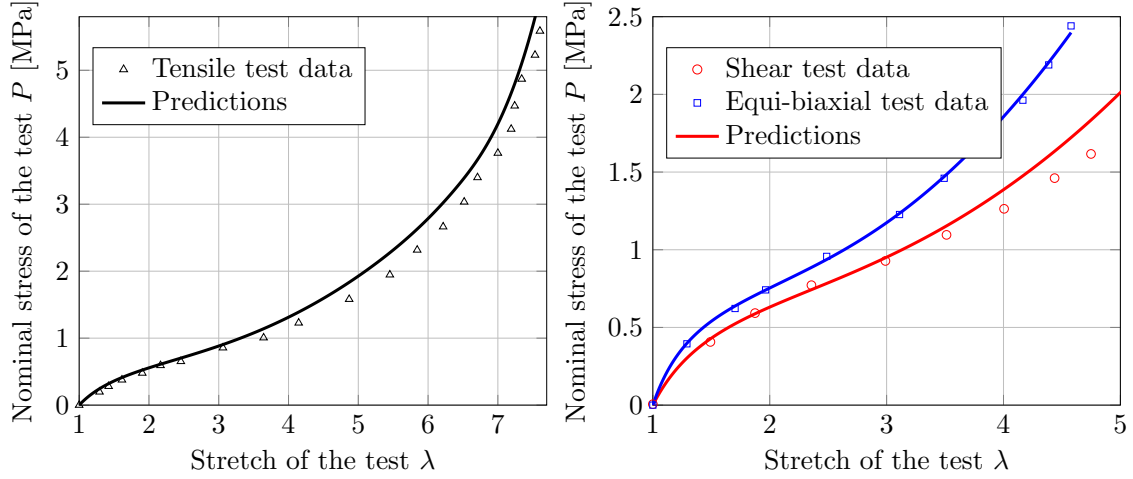


Figure 11: Predictions of Treloar's tests using  $P_{ch}$  captured from a biaxial test and extended with a rational function

to account for a limit stretch  $\lambda_{lock}$  and a proper continuity with the experimental part given by the constants  $a$  and  $b$ . The B-spline  $P_{ch}(\lambda_{ch})$  function has been thereafter used to predict the three Treloar tests, shown in Fig. 11, where we note that the equibiaxial test is predicted accurately, but the predictions of the uniaxial and pure shear tests have a larger error because the extrapolation employed is not directly based on experimental data.

A second option is to cover the domain using  $P_{ch}(\lambda_{ch})$  data from two of Treloar's tests. This approach is shown in Fig. 12. In this figure it is observed that the domain reached by the equibiaxial test and by the uniaxial test are different, and that in the common domain, data is similar, although not identical. A regression smooth B-spline of all data from both tests is employed to create a  $P_{ch}(\lambda_{ch})$  function that covers all the needed domain to predict Treloar's tests. These predictions are shown in Fig. 13, where it is clearly observed that in this case the equibiaxial test predictions are slightly less accurate, but the predictions for the other two tests have improved.

#### 4.3. Prediction of the Kawabata experiments using $P_{ch}(\lambda_{ch})$ from a Treloar material

In Section 4.1 we have shown that if the  $P_{ch}(\lambda_{ch})$  function representing the behavior of a typical chain in the Kawabata material is known, we are able to build the constitutive manifolds that accurately predict the behavior of the material under any loading condition. Following Khiêm and Itskov, we will use the  $P_{ch}(\lambda_{ch})$  function of Fig. 12 to predict the Kawabata experiments to investigate to what extent both the Treloar and the Kawabata materials behave in a similar way.

In Figs. 14 to 17 we show the predictions of the Kawabata experiments using Treloar's material. We show both the longitudinal nominal stress curves  $P_2(\lambda_2)$  and the transverse

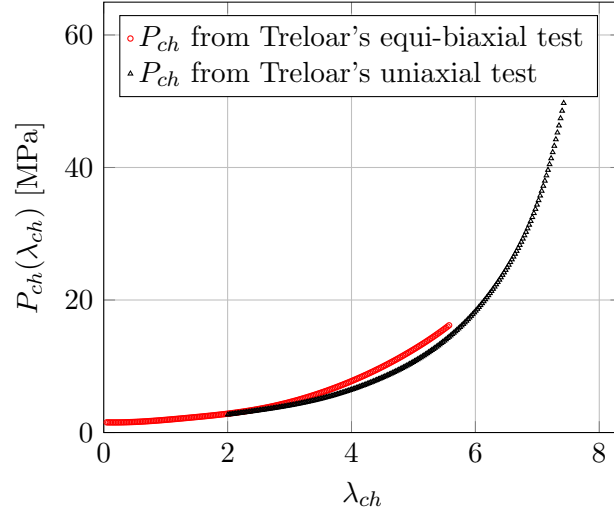


Figure 12:  $P_{ch}$  data obtained from the uniaxial and equi-biaxial tests by Treloar and final adopted B-spline curve. Note that the domain reached by both tests is different. Note also that in the overlapping part of the domain, the data obtained is very similar (although not identical).

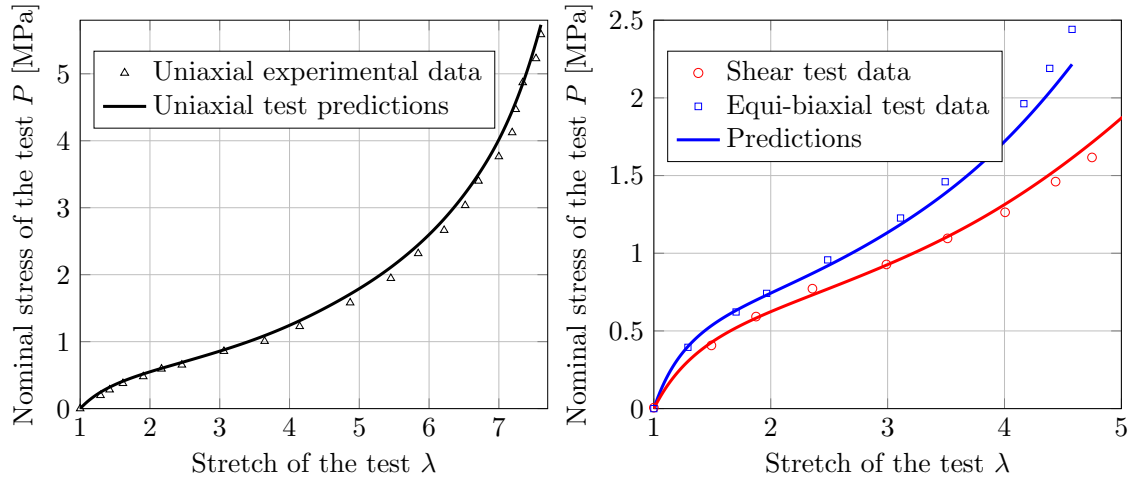


Figure 13: Predictions for Treloar's tests using a  $P_{ch}(\lambda_{ch})$  obtained from tensile test data with the domain completed with some equibiaxial data

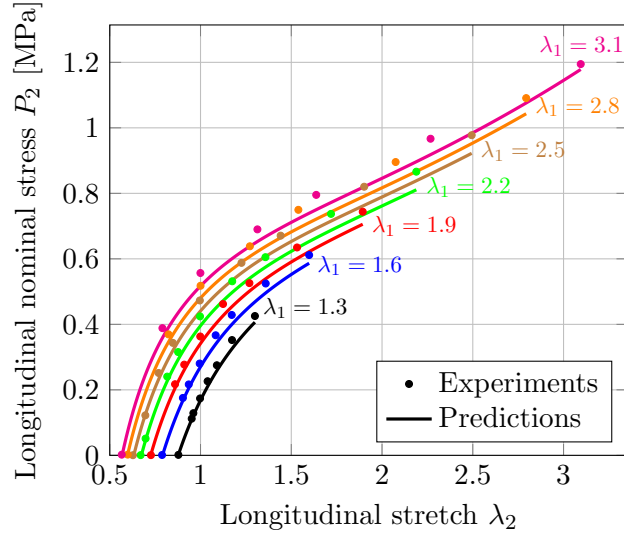


Figure 14: Predictions of  $P_2(\lambda_2)$  for the Kawabata experiments using  $P_{ch}(\lambda_{ch})$  from Treloar's material

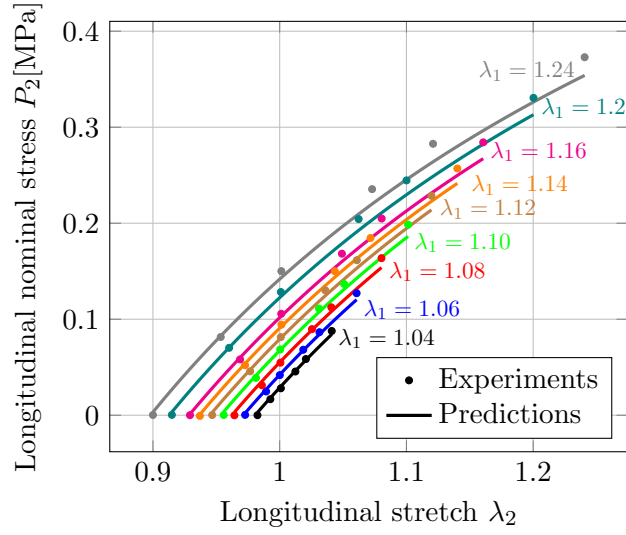


Figure 15: Predictions of  $P_2(\lambda_2)$  for the Kawabata experiments using  $P_{ch}(\lambda_{ch})$  from Treloar's material

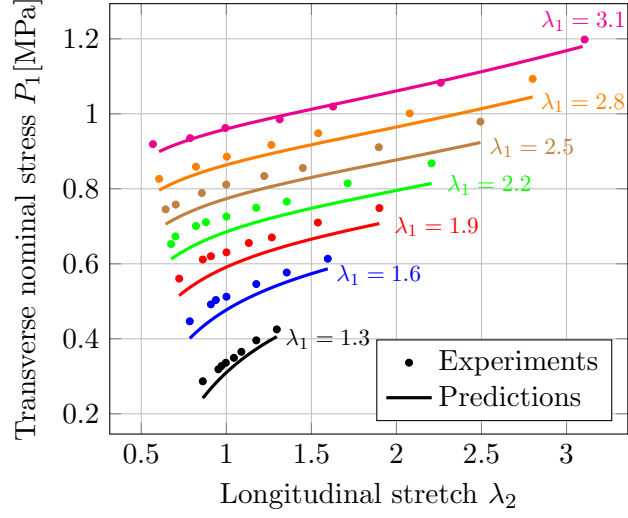


Figure 16: Predictions of  $P_1(\lambda_2)$  for the Kawabata experiments using  $P_{ch}(\lambda_{ch})$  from Treloar's material

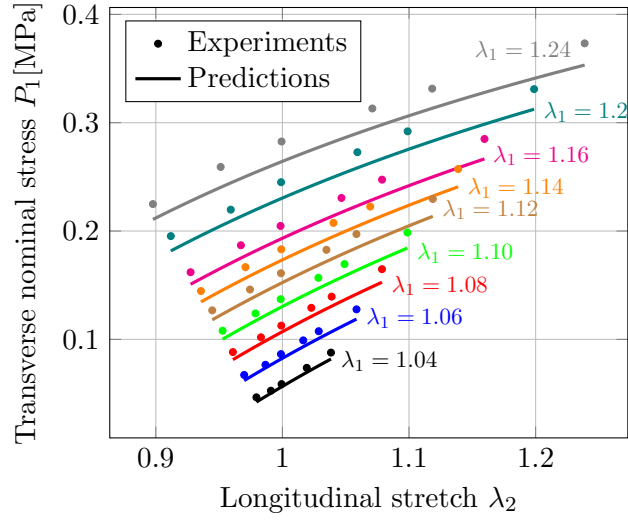


Figure 17: Predictions of  $P_1(\lambda_2)$  for the Kawabata experiments using  $P_{ch}(\lambda_{ch})$  from Treloar's material

nominal stress curves  $P_1(\lambda_2)$  for the different values of transverse stretch  $\lambda_1$ . These figures should be compared to Figs. 6 to 9. It is clearly observed that both materials are indeed similar, but not identical, because the present predictions are slightly worse than those shown in Figs. 6 to 9. The small but appreciable differences are indeed manifest in transverse stresses  $P_1(\lambda_2)$ . We note that using  $P_{ch}(\lambda_{ch})$  from Figs. 10 and 12 the same conclusion is obtained (differences using either curve are very small).

## 5. Conclusions

In this paper we have introduced a new data-driven structure-based procedure to model isotropic, rubber-like materials. The approach is a macro-micro-macro approach in the sense that the micromechanical behavior of the fibers is obtained, including all the interactions, directly from macroscopic tests solving a linear system of equations. This micromechanical behavior may be subsequently employed to build macroscopic constitutive manifolds to efficiently predict the behavior of the continuum via finite elements under any loading condition. We have applied the approach to predict, to very good accuracy, the series of biaxial tests from Kawabata et al. using only one of the tests to obtain the behavior of a representative fiber. We have also applied the procedure to obtain the behavior of a representative fiber in Treloar's material. This fiber behavior has subsequently been used to predict both Treloar's tests and Kawabata's biaxial test series. It is seen that whereas both materials are very similar, some differences may be appreciated in their behavior.

The present approach is nonparametric, and micro-mechanical assumptions about the behavior of the material are reduced to a minimum, but excellent accuracy is still obtained because the structure of the material (isotropic distribution of fibers) is accounted for. Therefore, the macro-micro-macro approach looks promising for reverse-engineering other types of materials as, for example, biological tissues.

## References

- [1] J. E. Mark, B. Erman, Rubberlike elasticity: a molecular primer, Cambridge University Press, 2007.
- [2] J. M. Benítez, F. J. Montáns, The mechanical behavior of skin: Structures and models for the finite element analysis, *Computers & Structures* 190 (2017) 75–107.
- [3] K.-J. Bathe, Finite element procedures, 2nd Ed., Klaus-Jürgen Bathe, 2014.
- [4] L. R. G. Treloar, The physics of rubber elasticity, Oxford University Press, USA, 1975.
- [5] J. S. Bergström, Mechanics of solid polymers: theory and computational modeling, William Andrew, 2015.



- [6] R. Ibañez, D. Borzacchiello, J. V. Aguado, E. Abisset-Chavanne, E. Cueto, P. Ladevèze, F. Chinesta, Data-driven non-linear elasticity: constitutive manifold construction and problem discretization, *Computational Mechanics* 60 (5) (2017) 813–826.
- [7] R. Ibáñez, E. Abisset-Chavanne, D. González, J.-L. Duval, E. Cueto, F. Chinesta, Hybrid constitutive modeling: data-driven learning of corrections to plasticity models, *International Journal of Material Forming* (2018) 1–9.
- [8] R. Ibanez, E. Abisset-Chavanne, J. V. Aguado, D. Gonzalez, E. Cueto, F. Chinesta, A manifold learning approach to data-driven computational elasticity and inelasticity, *Archives of Computational Methods in Engineering* 25 (1) (2018) 47–57.
- [9] T. Sussman, K.-J. Bathe, A model of incompressible isotropic hyperelastic material behavior using spline interpolations of tension–compression test data, *Communications in Numerical Methods in Engineering* 25 (1) (2009) 53–63.
- [10] M. Latorre, F. J. Montáns, Extension of the Sussman–Bathe spline-based hyperelastic model to incompressible transversely isotropic materials, *Computers & Structures* 122 (2013) 13–26.
- [11] M. Latorre, F. J. Montáns, What-You-Prescribe-is-What-You-Get orthotropic hyperelasticity, *Computational Mechanics* 53 (6) (2014) 1279–1298.
- [12] J. Crespo, M. Latorre, F. J. Montáns, WYPiWYG hyperelasticity for isotropic, compressible materials, *Computational Mechanics* 59 (1) (2017) 73–92.
- [13] J. Crespo, F. J. Montáns, A continuum approach for the large strain finite element analysis of auxetic materials, *International Journal of Mechanical Sciences* 135 (2018) 441–457.
- [14] M. Latorre, M. Mohammadkhah, C. K. Simms, M. F. J., A continuum model for tension-compression asymmetry in skeletal muscle, *Journal of the mechanical behavior of biomedical materials* 77 (2018) 455–460.
- [15] E. De Rosa, M. Latorre, F. J. Montáns, Capturing anisotropic constitutive models with WYPiWYG hyperelasticity; and on consistency with the infinitesimal theory at all deformation levels, *International Journal of Non-Linear Mechanics* 96 (2017) 75–92.
- [16] M. Latorre, F. J. Montáns, Experimental data reduction for hyperelasticity, *Computers & Structures* (in press, doi: 10.1016/j.compstruc.2018.02.011).
- [17] E. M. Arruda, M. C. Boyce, A three-dimensional constitutive model for the large stretch behavior of rubber elastic materials, *Journal of the Mechanics and Physics of Solids* 41 (2) (1993) 389–412.

- [18] L. Treloar, Stress-strain data for vulcanized rubber under various types of deformation, *Rubber Chemistry and Technology* 17 (4) (1944) 813–825.
- [19] C. Miehe, S. Göktepe, F. Lulei, A micro-macro approach to rubber-like materials—part I: the non-affine micro-sphere model of rubber elasticity, *Journal of the Mechanics and Physics of Solids* 52 (11) (2004) 2617–2660.
- [20] M. Kaliske, G. Heinrich, An extended tube-model for rubber elasticity: statistical-mechanical theory and finite element implementation, *Rubber Chemistry and Technology* 72 (4) (1999) 602–632.
- [21] V. N. Khiêm, M. Itskov, Analytical network-averaging of the tube model: Rubber elasticity, *Journal of the Mechanics and Physics of Solids* 95 (2016) 254–269.
- [22] K. Urayama, An experimentalist’s view of the physics of rubber elasticity, *Journal of Polymer Science Part B: Polymer Physics* 44 (24) (2006) 3440–3444.
- [23] S. Kawabata, M. Matsuda, K. Tei, H. Kawai, Experimental survey of the strain energy density function of isoprene rubber vulcanizate, *Macromolecules* 14 (1) (1981) 154–162.
- [24] M. Shariff, Strain energy function for filled and unfilled rubberlike material, *Rubber chemistry and technology* 73 (1) (2000) 1–18.
- [25] V. J. Amores, J. M. Benítez, F. J. Montáns, Average-chain behavior of isotropic incompressible polymers obtained from macroscopic experimental data. A simple structure-based WYPiWYG model in Julia language, *Advances in Engineering Software*, (in press, doi: 10.1016/j.advengsoft.2019.01.004).
- [26] A. Ammar, Effect of the inverse Langevin approximation on the solution of the fokker–planck equation of non-linear dilute polymer, *Journal of Non-Newtonian Fluid Mechanics* 231 (2016) 1–5.
- [27] A. N. Nguesong, T. Beda, F. Peyraut, A new based error approach to approximate the inverse Langevin function, *Rheologica Acta* 53 (8) (2014) 585–591.
- [28] M. Kröger, Simple, admissible, and accurate approximants of the inverse Langevin and Brillouin functions, relevant for strong polymer deformations and flows, *Journal of Non-Newtonian Fluid Mechanics* 223 (2015) 77–87.
- [29] M. Itskov, R. Dargazany, K. Hörnes, Taylor expansion of the inverse function with application to the Langevin function, *Mathematics and Mechanics of Solids* 17 (7) (2012) 693–701.
- [30] R. Jedynak, New facts concerning the approximation of the inverse Langevin function, *Journal of Non-Newtonian Fluid Mechanics* 249 (2017) 8–25.

- [31] B. C. Marchi, E. M. Arruda, An error-minimizing approach to inverse Langevin approximations, *Rheologica Acta* 54 (11-12) (2015) 887–902.
- [32] E. Darabi, M. Itskov, A simple and accurate approximation of the inverse Langevin function, *Rheologica Acta* 54 (5) (2015) 455–459.
- [33] J. M. Benitez, F. J. Montáns, A simple and efficient numerical procedure to compute the inverse langevin function with high accuracy, *Journal of Non-Newtonian Fluids Mechanics* 261 (2018) 153–163.
- [34] E. Riande, R. Diaz-Calleja, M. Prolongo, R. Masegosa, C. Salom, *Polymer viscoelasticity: stress and strain in practice*, CRC Press, 1999.
- [35] H. M. James, E. Guth, Theory of the elastic properties of rubber, *The Journal of Chemical Physics* 11 (10) (1943) 455–481.
- [36] R. L. Anthony, R. H. Caston, E. Guth, Equations of state for natural and synthetic rubber-like materials. i. unaccelerated natural soft rubber, *The Journal of Physical Chemistry* 46 (8) (1942) 826–840.
- [37] D. J. Williams, *Polymer science and engineering*, Prentice-Hall international series in the physical and chemical engineering sciences, 1971.
- [38] P. Bažant, B. Oh, Efficient numerical integration on the surface of a sphere, *ZAMM-Journal of Applied Mathematics and Mechanics/Zeitschrift für Angewandte Mathematik und Mechanik* 66 (1) (1986) 37–49.
- [39] H. L. Weinert, *Fast compact algorithms and software for spline smoothing*, Springer, 2013.
- [40] P. H. Eilers, B. D. Marx, Flexible smoothing with b-splines and penalties, *Statistical Science* (1996) 89–102.
- [41] F. O’Sullivan, B. S. Yandell, W. J. Raynor Jr, Automatic smoothing of regression functions in generalized linear models, *Journal of the American Statistical Association* 81 (393) (1986) 96–103.
- [42] R. L. Eubank, *Nonparametric regression and spline smoothing*, CRC press, 1999.